Microchimica Acta (2022) 189: 105
https://doi.org/10.1007/s00604-022-05210-y

ORIGINAL PAPER

Electrochemical biosensing of circulating microRNA-21 in cerebrospinal fluid of medulloblastoma patients through target-induced redox signal amplification

Chen Wang[1] · Yujie Liu[2] · Ruoping Chen[1] · Xiaoqiang Wang[1] · Yunkun Wang[1] · Jia Wei[1] · Kun Zhang[2] · Chenran Zhang[1]

Received: 16 November 2021 / Accepted: 30 January 2022 / Published online: 14 February 2022

Abstract

Monitoring of cerebrospinal fluid (CSF) microRNAs (miRs) offers a promising option for the diagnosis and management of patients with central nervous system tumors. However, the sensitive detection of miRs in clinical CSF samples has been hindered by the ultra-low abundance of target miRs. Here, we report an electrochemical biosensor for the highly sensitive label-free detection of CSF miR-21 relying on target-induced redox signal amplification (eTIRSA). The biosensor was developed by covalently assembling the capture stands partially complementary to miR-21 on the gold nanoparticle-coated glassy carbon electrode. In the presence of miR-21, the short capture stand hybridized with the partial bases of miR-21, allowing the rest sequence of the target molecule to further bind with a long guanine-rich sequence which could specifically adsorb a number of methylene blue indicators, thus generating an amplified electrochemical redox signal, typically at a working potential of − 0.19 V (vs. SCE). The response of the surface-bound methylene blue indicators was positively correlated to the concentration of miR-21, providing a dynamic range of 0.5–80 pM and a limit of detection down to 56 fM. Moreover, the eTIRSA biosensor had high specificity with single-base resolution and exhibited good performance for label-free quantification of miR-21 in medulloblastoma cell extracts and clinical CSF samples and for accurate discrimination of medulloblastoma against non-cancer controls, indicating its potential application in CSF miR-based liquid biopsy of brain cancers.

Keywords Electrochemical biosensor · MicroRNA · Cerebrospinal fluid · Medulloblastoma · Target-induced signal amplification

Introduction

Central nervous system (CNS) tumors are the most prevalent solid tumor malignancy in children [1]. Despite substantial advances in diagnosis and treatment [2], these diseases remain the leading cause of cancer death and severe functional deficits in children [3, 4]. Timely diagnosis is critical to an improved clinical outcome of patients with CNS tumors [5, 6]. Although neuroimaging and tissue biopsy have been used for the diagnosis of CNS tumors, these techniques suffer from either insufficient sensitivity or invasiveness [7]. Furthermore, tissue biopsy may subject to sampling bias due to the intratumor heterogeneity [7, 8]. Thus, reliable noninvasive methods are desirable to diagnose and monitor the cause of CNS tumors.

The liquid biopsy of cerebrospinal fluid (CSF) offers an attractive alternative for the management of CNS tumors by analyzing circulating tumor-associated molecular clues in a minimally invasive manner [9–11]. CSF interacts directly with brain malignancies and has been proven to contain multiple circulating biomarkers in the occurrence and progress of CNS tumors [12, 13]. Accumulating evidence implicates that the abnormal levels of CSF microRNAs (miRNAs) are associated with malignant CNS tumors [14–16]. The molecular profile of CSF miRNAs has been demonstrated to

✉ Kun Zhang
kunzhang@shsmu.edu.cn

✉ Chenran Zhang
zhangchenran@xinhuamed.com.cn

[1] Department of Pediatric Neurosurgery, Xinhua Hospital, Shanghai Jiao Tong University School of Medicine, Shanghai 200092, China

[2] Shanghai Institute of Pediatric Research, Shanghai Key Laboratory of Pediatric Gastroenterology and Nutrition, Xinhua Hospital, Shanghai Jiao Tong University School of Medicine, Shanghai 200092, China

possess multiple abilities for distinguishing different types of brain cancers [14, 17], tracking disease status [18], and evaluating drug resistance [19]. In addition, abnormal miRNA expression is often an early event in tumorigenesis; the quantitative analysis of their abundance in clinical CSF is, therefore, beneficial to the early cancer diagnostic. However, the reliable and sensitive detection of miRNAs in complex biofluids such as CSF remains challenging because of their low concentration, short sequence length, and high homology [20]. The "gold standard" reverse transcription polymerase chain reaction (RT-PCR) and sequencing tests for miRNA are accurate [21] but are costly and need elaborate sample processing [22]. Alternatively, the microarray analysis has an insufficient selectivity and narrow dynamic range [23, 24]. To circumvent these limitations, several PCR-free biosensors have been developed for in vitro and in vivo miRNA detection with improved sensitivity, although at the expense of sophisticated probe design and fabrication (e.g., use of multiple primers [25] or enzymes [26–28], synthesis of ultrasensitive nanoprobes [29–33]).

Electrochemical biosensors hold promise for clinical miRNA detection because of the merits of low cost, simple operation, and fast response [34–36]. The typical analysis of miRNAs associates with the measurement of the change in electrochemical signal resulting from the binding of the miRNA target on the biosensing interface. To evaluate hybridization between the target miRNA and the complementary probe strand, either a labeling or label-free strategy is commonly used. In contrast to the labeling-based detection, the label-free electrochemical assay of miRNAs directly detects the hybridization process on an electrode surface by using a suitable electrochemical redox indicator such as methylene blue [37]. As a kind of phenothiazine, methylene blue interacts strongly with the unbound guanine (G) bases mainly through the noncovalent intercalation due to its planer structure [38]. However, most reported electrochemical miRNA biosensors employ methylene blue to directly bind to the formed double-stranded oligonucleotides after target capture [39]. The short sequence length and limited numbers of guanine bases (both dependent on the sequence of the target miRNA) inevitably cause an insufficient binding of the indicator; additional electrode modifications are thereby needed to enhance the signal readout.

In this work, we present a simple yet efficient miRNA electrochemical biosensor capable of highly sensitive detection of miRNA-21 in CSF of patients with medulloblastoma (MB) based on a target-induced electrochemical redox amplification (eTIRSA) mechanism. MB is the most common and malignant pediatric brain tumor [40, 41]. The up-regulation of miRNA-21 has been found both in human primary MB and in MB cell lines [42]. Here, we used a short partial complemented probe DNA to capture the target miRNA-21 and a 50-nt guanine-rich single-stranded DNA to boost the adsorption of the methylene blue indicator on the electrode surface, thus to improve the assay sensitivity. As shown, only in the presence of miRNA-21, an intense and amplified electrochemical redox signal of methylene blue was recorded. Our eTIRSA-based biosensing scaffold provides the ability to specifically recognize miRNA-21 at the femtomolar level and single-base resolution, to reliably quantify the circulating miRNA-21 in clinical CSF, and to discriminate MB from the non-cancer control based on the CSF miRNA signature.

Experimental

Chemicals and materials

The DNA sequences and miRNAs were synthesized and provided by Sangon Biotech (Shanghai, China). All oligonucleotides were purified by HPLC, and their sequences were listed in Table s1. Fetal bovine serum (FBS), penicillin–streptomycin solution, Minimum Essential Medium (MEM), and Dulbecco's Modified Eagle Medium (DMEM) were purchased from Gibco (Carlsbad, CA). Tetrachloroauric(III) acid tetrahydrate chloroauric acid ($HAuCl_4{\cdot}4H_2O$), potassium dihydrogen phosphate (KH_2PO_4), disodium hydrogen phosphate (K_2HPO_4), sodium chloride (NaCl), potassium chloride (KCl), potassium nitration (KNO_3), potassium ferricyanide ($K_3Fe(CN)_6$), and potassium ferrocyanide trihydrate ($K_4Fe(CN)_6{\cdot}3H_2O$) were purchased from Sinopharm (Shanghai, China). Diethylpyrocarbonate (DEPC) was purchased from Merck (Shanghai, China). All aqueous solutions were prepared with Milli-Q water (18.2 MΩ cm) and treated with DEPC to minimize the effect of RNases. For the same purpose, all the sample tubes, microchips, and glassware were autoclaved before use.

Apparatus and measurements

A CHI1240C electrochemical analyzer (Chen Hua Instrument, Shanghai) with a three-electrode system was employed for the cyclic voltammetric (CV) and differential pulse voltammetric (DPV) measurements. A bare or gold nanoparticle-coated glassy carbon electrode (GCE, Ø = 3.0 mm) was used as the working electrode, a platinum wire was used as the auxiliary electrode, and a saturated calomel electrode (SCE) was used as the reference electrode. All potentials were referenced to SCE. CV was carried out at a potential window of − 0.2 to 0.6 V with a scan rate of 100 mV/s. DPV was performed in 10 mM PBS (pH 7.4) using a potential range from − 0.6 V to 0.2 V, pulse amplitude 0.05 V, pulse width 0.05 s, and sample interval 0.002 s. Electrochemical impedance spectroscopy (EIS) was performed using a PGSTAT 302 N system (Metrohm Autolab, Switzerland) at

a potential of 0.2 V vs SCE over the frequency range from 0.1 Hz to 100 kHz. A solution mixture containing 5.0 mM $[Fe(CN)_6]^{3-/4-}$ and 0.1 M KCl was used as the supporting electrolyte.

Polyacrylamide gel electrophoresis

The hybridization process was analyzed on 10% native PAGE gel. Initially, the capture probe (Cp) and auxiliary strand were dissolved in 10 mM PBS solution (pH 7.4, 1 M NaCl), respectively. Subsequently, the capture strand solution was mixed with miR-21 and incubated at 37 ℃ for 1 h. After that, the auxiliary strand was added to the solution mixture and incubated at 37 ℃ for another 1 h. The gel was run in 1 × TAE (Tris–acetic acid-EDTA) buffer at 115 V for 90 min. After electrophoresis on a Tanon VE-180C vertical electrophoresis system (Tanon, Inc., China), the gels were visualized with 3 × GelRed stain and scanned by a Chemi DocTM Touch imaging system (Bio-Rad Laboratories, USA).

eTIRSA biosensor for miR-21 detection

The GCE surface was first polished with 0.5 and 0.05 μm alumina slurries and washed successively with ethanol and water. Then, the GCE was immersed in 0.1% $HAuCl_4$ solution containing 0.1 M KNO_3. AuNPs were electrodeposited on the GCE electrode by applying a fixed potential at − 0.2 V for 90 s. Subsequently, 10 μL capture strand solution (0.1 μM) was dropped onto the electrode followed by incubation overnight at room temperature. The electrode was further incubated in 1% BSA for 1 h to block the nonspecific binding sites. Then, the electrode was incubated with 10 μL of the miR-21 solution at 37 ℃ for 1 h. After thorough washing, 10 μL auxiliary DNA solution (0.1 μM) was added on the electrode, followed by incubation at 37 °C for 1 h and triplet washing with 10 mM PBS solution. Finally, 8 μL methylene blue aqueous solution (1 mM) was dropped on the electrode surface for 1 h to allow sufficient binding. After thorough washing with PBS, the electrode was subjected to electrochemical analysis at the conditions described above. The current values acquired at a working potential of − 0.19 V (vs SCE) were plotted against the miR-21 concentrations to build the calibration curve.

Cell culture

The human microglial cells (HMC3) were purchased from FuHeng Biology Co., Ltd (Shanghai, China). The DAOY cells were purchased from the Shanghai Cell Bank of the Chinese Academy of Sciences (Shanghai, China). The DAOY cells were cultured in DMEM high-glucose medium supplemented with 10% FBS, 1% sodium pyruvate, and penicillin–streptomycin. The HMC3 cells were cultured in MEM. Cells were maintained at 37 °C in a humidified atmosphere containing 5% CO_2. For the cellular RNA extraction, the DAOY cells and HMC3 cells were plated in 6-well-plate for 48 h. Then, total RNA was then extracted using TRIzol™ reagent (Takara, Dalian, China) in accordance with the manufacturer's protocol.

Clinical CSF sample collection, processing, and detection

CSF samples of MB patients and hydrocephalus patients (non-cancer controls) were collected at Xinhua Hospital, Shanghai Jiao Tong University School of Medicine, which was approved by the Ethics Committee of the hospital (XHEC-D-2021–087). The detail information of patients was summarized in Table s2. Written informed consent was obtained from all the participants before sample acquisition. Freshly collected CSF samples were centrifuged at 1000 g for 10 min, then divided into aliquots, and stored immediately at − 80 °C before use. For the detection of miR-21, 1 μl of cerebrospinal fluid was diluted 40-fold with 10 mM PBS. Then, 10 μL of the diluted sample was subjected to analysis with above procedures. Again, the DPV signal at the working potential of − 0.19 V (vs SCE) was extracted and analyzed.

Results and discussion

Working principle of the eTIRSA biosensor

Scheme 1 illustrates the working principle of the eTIRSA biosensor for highly sensitive detection of miR-21 in clinical CSF. Initially, a thiol-terminated short single-strand DNA (11 nt) serving as the Cp was immobilized on the AuNPs-coated GCE surface. In the presence of miR-21 (22 nt), the Cp hybridized with partial bases of the target miR-21 and allowed the rest sequence of miR-21 to bind a long guanine-rich auxiliary DNA strand (50 nt) through base stacking hybridization. It has been proved that the guanine-rich sequence has a favored binding with methylene blue, an electrochemical redox-active phenothiazine dye, and this may contribute to the formation of tetramolecular G-quadruplex structure.[43] An intense electrochemical response can therefore be observed at the electrode surface owing to redox of the large quantities of adsorbed methylene blue indicators. In contrast, when miR-21 is absent, the specific hybridization does not execute, thereby the electrochemical signal is fairly weak. Compared with conventional DNA biosensors using an oligonucleotide sequence labeled with a single dye (e.g., methylene blue) as the signal reporter, our eTIRSA sensor, once activated by the target miRNA, leverages a long

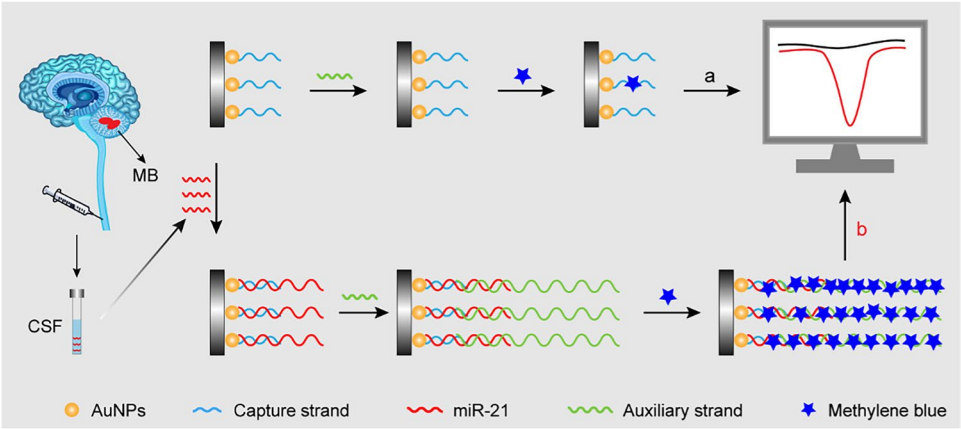

Scheme 1 Schematic diagram of a target-induced redox signal amplification (TIRSA)-based electrochemical (eTIRSA) biosensor for the detection of circulating CSF miR-21

DNA sequence capable of specifically adsorbing many methylene blue molecules, which largely amplifies the detection signal (Fig. s1).

Design of the eTIRSA biosensor

To prove the above assembly mechanism (Fig. 1a), we first carried out a PAGE experiment to analyze the hybridization for different combinations of the three oligonucleotides. As shown in Fig. 1b, only the simultaneous presence of the target miR-21, the Cp, and the auxiliary strand resulted in an oligonucleotide assembly with the most slowly electrophoretic mobility. DPV tests were then performed to characterize the property of the electrode following stepwise interfacial engineering. As displayed in Fig. s2, a significant DPV signal of methylene blue appeared when Cp and miR-21 (curve ii) were applied on AuNPs/GCE because the methylene blue molecules were strongly adsorbed by the guanine units on the exposed Cp and miR-21. When auxiliary DNA was immobilized on the miR-21/BSA/Cp/AuNPs/GCE, the

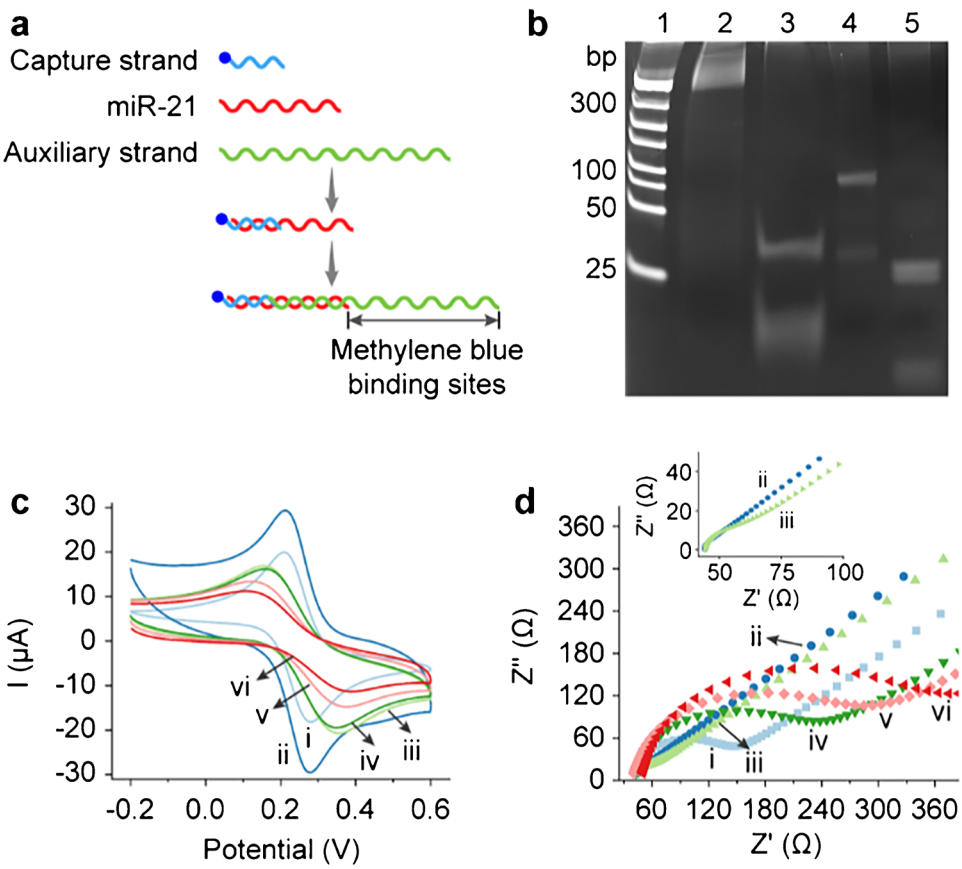

Fig. 1 **a** Target miR-21-induced ligation of the capture strands and the auxiliary strands via complementary base pairing. **b** Gel electrophoresis image of the capture strand-miR-21-auxiliary strand assembly and the corresponding different sequence combinations: lane 1, marker; lane 2, capture strand + miR-21 + auxiliary strand; lane 3, miR-21 + auxiliary strand; lane 4, auxiliary strand; lane 5, capture strand. **c** CV and **d** EIS curves measured after stepwise modification of the electrode surface: i, bare GCE; ii, AuNPs/GCE; iii, Cp/AuNPs/GCE; iv BSA/Cp/AuNPs/GCE; v, miR-21/ BSA/Cp/AuNPs/GCE; and vi, auxiliary strand/ miR-21/ BSA/Cp/AuNPs/GCE. Insert showing the detail of the curves ii and iii

partial hybridization of auxiliary DNA and miR-21 led to an obvious increase of DPV response of methylene blue (curve iv), which was about 2 times higher than that of the Cp/AuNPs/GCE, indicating remarkable signal amplification of the hybridization reaction.

Feasibility characterization of the electrochemical biosensor

The biosensor was then characterized by electrochemical CV measurements, which provided more prolific information about the change of interface property of the microRNA modified electrode since the decrease of redox peak was equal to the increase of the interfacial electrons transfer resistance. Figure 1c shows the CV obtained in 0.1 mM $Fe(CN)_6^{3-/4-}$ solution containing 0.1 M KCl at different electrodes. AuNPs modified GCE electrode exhibited a higher current redox peak of $Fe(CN)_6^{3-/4-}$ (curve ii) with an enhanced electron transfer than bare GCE (curve i). After the thiolated Cp was self-assembled onto the electrode surface, the current redox peak of $Fe(CN)_6^{3-/4-}$ decreased significantly (curve iii). When the electrode was treated with 1% BSA to block the non-specific adsorption sites and then immersed in 0.1 μM miR-21, the current voltammogram redox peak of $Fe(CN)_6^{3-/4-}$ further decreased (curves iv and v) due to the steric hindrance of electron transfer after miR-21 was hybridized with Cp. When auxiliary DNA hybridized with miR-21, the current voltammogram redox peak of $Fe(CN)_6^{3-/4-}$ further decreased (curve vi).

The detailed change in electron-transfer resistance (Ret) can be further detected by EIS. Figure 1d shows the impedance spectra of the interfaces recorded after each modification step. Due to the good electric charge transferability, the AuNPs modified GCE (curve ii) displayed an almost straight line in the Nyquist plot, exhibiting a lower Ret than the bare GCE (curve i). It was clear that the diameter of the semicircles successively increased with the sequential assembly of Cp (curve iii), BSA (curve iv), miR-21 (curve v), and auxiliary DNA (curve vi), indicating a gradual increase in the Ret step by step. These results were well consistent with the phenomena in CVs, confirming the successful preparation of the biosensor.

Detection performance of the eTIRSA biosensor

Under the optimized conditions (Fig. s4), we next evaluated the assay performance of the proposed eTIRSA sensor by detecting miR-21 in 10 mM PBS with DPV. Figure 2a shows the DPV curves of solutions containing varied concentrations of miR-21 from 0 to 100 pM. The signal increased monotonically along with the rising concentration of miR-21(Fig. 2b). The corresponding calibration plot of the current change (ΔI) against the logarithm of miR21 concentrations exhibited a good linearity with a dynamic range from 0.5 to 80 pM (Fig. 2c). The associated linear regression equation was $\Delta I = 1.39\ \lg C + 15.188$ with a correlation coefficient (R^2) of 0.991. The limit of detection was estimated to be 56 fM (signal-to-noise ratio,

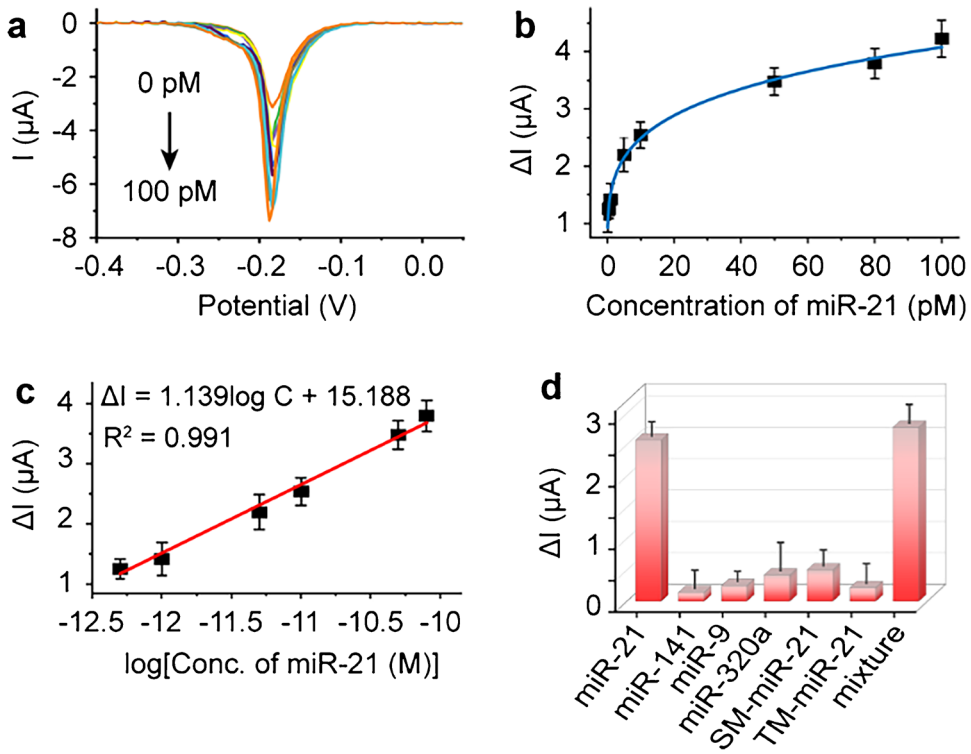

Fig. 2 **a** DPV curves determined from different concentrations of miR-21. **b** Changes of the redox current values (ΔI) as a function of different concentrations of miR-21 from 0.1 pM to 100 pM. **c** Linear correlation between ΔI and the logarithm of target concentrations. **d** Response of the eTIRSA sensor to miR-21, miR-141, miR-9, miR-320a, single-mismatched sequence, three-mismatched sequence, and mixture of miR-21 and the above miRNAs. The concentration of miR21 is 0.01 nM and that of other sequecens is 1 nM

SNR = 3). Moreover, compared to other reported methods leveraging enzymatic catalysis or advanced nanomaterials to boost the electrochemical signal (Table s3), the proposed biosensor showed a comparable detection performance for miR-21 but was more cost-effective and user-friendly, which could be attributed to the target-induced binding and enrichment of methylene blue to the G-rich strands with an enhanced redox response.

We next evaluated the selectivity of the eTIRSA biosensor by measuring the response current of solutions containing the fully matched (miR-21), single-base mismatched (SM-miR-21), three-base mismatched (TM-miR-21), and random microRNA (miR-14) sequences, respectively (Fig. 2d). The current change (ΔI) generated by SM, TM, and miR141, miR-9, and miR-320a (0.1 nM) was 19.5%, 8.6%, and 5.6%, 9.7%, and 16.3% of that generated by the target miR-21 (10 pM). In addition, no apparent difference in the ΔI value was observed for miR-21 detection with and without the presence of the other sequences. This result clearly indicated that the eTIRSA biosensor had good selectivity to recognize the target microRNA with single-based resolution.

To evaluate the accuracy of the proposed biosensor for miR-21 detection, we next performed recovery experiments by adding miR-21 standards to three clinical CSF samples from patients with hydrocephalus (Table s4). The calculated percentage of recovery was observed in the range from 90.7 to 109.7% with the relative standard variation values ranging from 2.1 to 4.5%, implying that this biosensor had a high accuracy for the quantification of miR-21 levels in complex biofluids (e.g., CSF).

Cellular miR-21 detection

Having demonstrated the assay performance of the proposed biosensor for miR-21, we then turned our attention to its bioanalytical applications. To this end, we cultured the MB DAOY cells, extracted the total cellular RNAs, and analyzed the miR-21 concentration using the eTIRSA sensor. For comparison, the miR-21 concentration in HMC3 was also measured (Fig. 3a). The detected level of miR-21 extracted from the DAOY cells was discernably greater than that from the HMC3 cells (Fig. 3b), consistent with literature reports that the expression level of miR-21 was up-regulated in MB [18].

Detection of miR-21 in CSF of MB patients

Finally, we applied the eTIRSA sensor to detect miR-21 in CSF of MB patients ($n = 5$). CSF samples from patients with hydrocephalus were collected as a non-cancer negative control (NCC, $n = 5$). Figure 4a shows that the electrochemical signal in response to the CSF of MB patients was apparently higher than that of NCCs, indicating the elevated expression of CSF miR-21 in cancer patients. Figure 4b further demonstrates that there was a statistical difference in the expression levels of circulating CSF miR-21 between MB patients and NCCs; the patient samples could be well-distinguished from the non-cancerous ones ($p < 0.05$). This pre-clinical analysis not only confirmed that CSF miR-21 could serve as a potential cancer biomarker but also suggested that our eTIRSA sensor was a promising tool to enable liquid biopsy for non-invasive detection of malignant brain tumors.

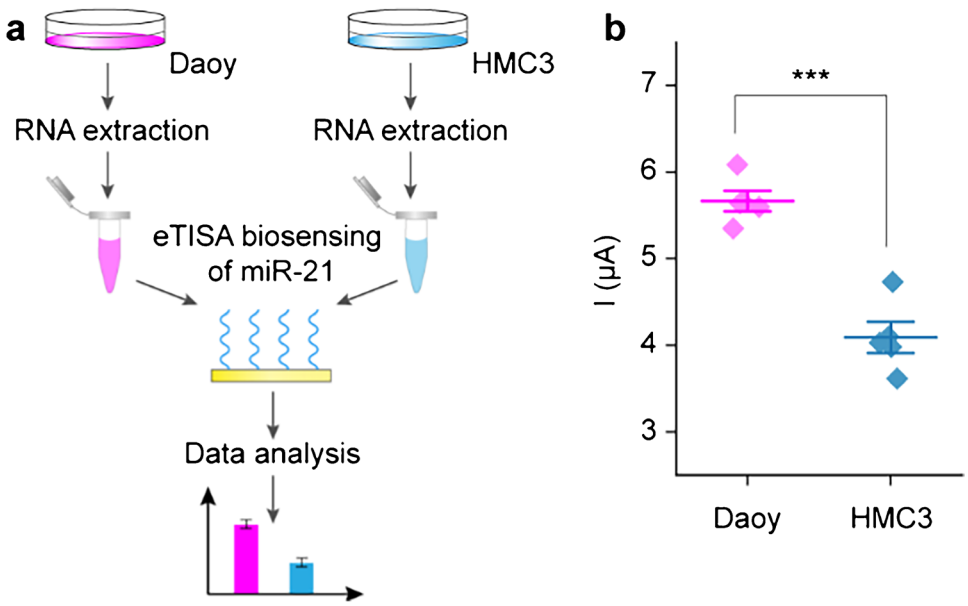

Fig. 3 **a** Schematic diagram of the detection of miR-21 from the MB Daoy cells and HMC3 cells. **b** Significant expression difference of miR-21 levels between the Daoy and HMC3 cells ($p < 0.001$)

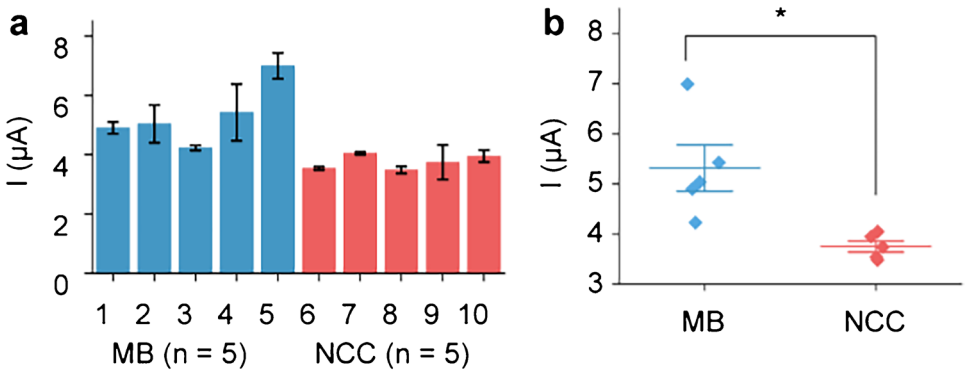

Fig. 4 **a** Using the eTIRSA biosensor to assay the target miR-21 concentration in circulating CSF samples of MB patients ($n=5$) and non-cancer controls ($n=5$). **b** Significant difference of miR-21 levels between MB patients and non-cancer controls (hydrocephalus, $p<0.05$)

Conclusion

In conclusion, we designed a simple yet highly sensitive electrochemical biosensor for the quantitative assay of circulating miR levels in clinical CSF samples based on the target-induced signal amplification (eTIRSA) mechanism. Although no other complex signal amplification strategies, such as rolling circle amplification and strand displacement amplification, were involved, our eTIRSA sensor was capable of detecting the miR target at low femtomolar levels with single-base resolution. Such a high sensitivity and specificity of the eTIRSA sensor allowed us to reliably measure the expression level of miR-21 in complex cell extracts, and more importantly, in clinical CSF samples of MB patients, offering a promising non-invasive technique tool to accurately distinguish MB patients and non-cancer controls. Future research will focus on further improvement of the detection limit by minimizing nonspecific adsorption events. In addition, by the combination of probe engineering and electrode modification, we expect that the eTIRSA biosensor can be further generalized for sensing other CSF miRs and be used in molecular detection and monitoring of brain cancers like MB by multiplexed CSF miR biopsy.

Supplementary Information The online version contains supplementary material available at https://doi.org/10.1007/s00604-022-05210-y.

Funding This work was financially supported by the National Natural Science Foundation of China (21974088 and 81500601), the Science and Technology Commission of Shanghai Municipality (21ZR1481300), and Hospital Funded Clinical Research-Clinical Research Unit-Xin Hua Hospital Affiliated to Shanghai Jiao Tong University School of Medicine (17CSY02). Components in Scheme 1 were created with vismatrix.cn, and the right to re-use the clip arts was purchased.

Declarations

Competing interests The authors declare no competing interests.

References

1. Louis DN, Ohgaki H, Wiestler OD, Cavenee WK, Burger PC, Jouvet A, Scheithauer BW, Kleihues P (2007) The 2007 WHO classification of tumours of the central nervous system. Acta Neuropathol 114:97–109. https://doi.org/10.1007/s00401-007-0243-4
2. Komori T (2017) The 2016 WHO classification of tumours of the central nervous system: the major points of revision. Neurol Med Chir 57:301–311. https://doi.org/10.2176/nmc.ra.2017-0010
3. Siegel RL, Miller KD, Jemal A (2019) Cancer statistics, 2019. CA Cancer J Clin 69:7–34. https://doi.org/10.3322/caac.21551
4. Ostrom QT, Cioffi G, Waite K, Kruchko C, Barnholtz-Sloan JS (2021) CBTRUS statistical report: primary brain and other central nervous system tumors diagnosed in the United States in 2014–2018. Neuro Oncol 23:iii1–iii105. https://doi.org/10.1093/neuonc/noab200
5. Frühwald MC, Rutkowski S (2011) Tumors of the central nervous system in children and adolescents. Dtsch Arztebl Int 108:390–397. https://doi.org/10.3238/arztebl.2011.0390
6. Zhang X, Zhou J, Gu Z, Zhang H, Gong Q, Luo K (2021) Advances in nanomedicines for diagnosis of central nervous system disorders. Biomaterials 269:120492. https://doi.org/10.1016/j.biomaterials.2020.120492
7. Ahmed R, Oborski MJ, Hwang M, Lieberman FS, Mountz JM (2014) Malignant gliomas: current perspectives in diagnosis, treatment, and early response assessment using advanced quantitative imaging methods. Cancer Manag Res 6:149–170. https://doi.org/10.2147/CMAR.S54726
8. Parikh AR, Leshchiner I, Elagina L et al (2019) Liquid versus tissue biopsy for detecting acquired resistance and tumor heterogeneity in gastrointestinal cancers. Nat Med 25:1415–1421. https://doi.org/10.1038/s41591-019-0561-9
9. Whitin JC, Jang T, Merchant M, Yu TT, Lau K, Recht B, Cohen HJ, Recht L (2012) Alterations in cerebrospinal fluid proteins in a presymptomatic primary glioma model. PLoS ONE 7:e49724. https://doi.org/10.1371/journal.pone.0049724
10. Khwaja FW, Reed MS, Olson JJ, Schmotzer BJ, Gillespie GY, Guha A, Groves MD, Kesari S, Pohl J, Van Meir EG (2007) Proteomic identification of biomarkers in the cerebrospinal fluid (CSF) of astrocytoma patients. J Proteome Res 6:559–670. https://doi.org/10.1021/pr060240z
11. Shen F, Zhang Y, Yao Y, Hua W, Zhang HS, Wu JS, Zhong P, Zhou LF (2014) Proteomic analysis of cerebrospinal fluid: toward the identification of biomarkers for gliomas. Neurosurg Rev 37:367–380. https://doi.org/10.1007/s10143-014-0539-5

12. Weston CL, Glantz MJ, Connor JR (2011) Detection of cancer cells in the cerebrospinal fluid: current methods and future directions. Fluids Barriers CNS 8:14. https://doi.org/10.1186/2045-8118-8-14
13. Shalaby T, Achini F, Grotzer MA (2016) Targeting cerebrospinal fluid for discovery of brain cancer biomarkers. J Cancer Metastasis Treat 2016:176–187. https://doi.org/10.20517/2394-4722.2016.12
14. Drusco A, Bottoni A, Laganà A, Acunzo M, Fassan M, Cascione L, Antenucci A, Kumchala P, Vicentini C, Gardiman MP, Alder H, Carosi MA, AmmiRati M, Gherardi S, Luscrì M, Carapella C, Zanesi N, Croce CM (2015) A differentially expressed set of microRNAs in cerebro-spinal fluid (CSF) can diagnose CNS malignancies. Oncotarget 6:20829–20839. https://doi.org/10.18632/oncotarget.4096
15. Baraniskin A, Chomiak M, Ahle G, Gress T, BuchholzTurewicz MM, Eisenacher M, Margold M, Schlegel U, Schmiegel W, Hahn S, Schroers R (2018) MicroRNA-30c as a novel diagnostic biomarker for primary and secondary B-cell lymphoma of the CNS. J Neurooncol 137:463–468. https://doi.org/10.1007/s11060-018-2749-0
16. Wang X, Holgado BL, Ramaswamy V, Mack S, Zayne K, Remke M, Wu X, Garzia L, Daniels C, Kenney AM, Taylor MD (2018) miR miR on the wall, who's the most malignant miR of them all? Neuro Oncol 20:313–323. https://doi.org/10.1093/neuonc/nox106
17. Baraniskin A, Kuhnhenn J, Schlegel U, Maghnouj A, Zöllner H, Schmiegel W, Hahn S, Schroers R (2012) Identification of microRNAs in the cerebrospinal fluid as biomarker for the diagnosis of glioma. Neuro Oncol 14:29–33. https://doi.org/10.1093/neuonc/nor169
18. Teplyuk NM, Mollenhauer B, Gabriely G, Giese A, Kim E, Smolsky M, Kim RY, Saria MG, Pastorino S, Kesari S, Krichevsky AM (2012) MicroRNAs in cerebrospinal fluid identify glioblastoma and metastatic brain cancers and reflect disease activity. Neuro Oncol 14:689–700. https://doi.org/10.1093/neuonc/nos074
19. Zeng A, Wei Z, Yan W, Yin J, Huang X, Zhou X, Li R, Shen F, Wu W, Wang X, You Y (2018) Exosomal transfer of miR-151a enhances chemosensitivity to temozolomide in drug-resistant glioblastoma. Cancer Lett 436:10–21. https://doi.org/10.1016/j.canlet.2018.08.004
20. Chevillet JR, Lee I, Briggs HA, He Y, Wang K (2014) Issues and prospects of microRNA-based biomarkers in blood and other body fluids. Molecules 19:6080–6105. https://doi.org/10.3390/molecules19056080
21. Varkonyi-Gasic E, Wu R, Wood M, Walton EF, Hellens RP (2007) Protocol: a highly sensitive RT-PCR method for detection and quantification of microRNAs. Plant Methods 3:12. https://doi.org/10.1186/1746-4811-3-12
22. Chen C, Ridzon DA, Broomer AJ, Zhou Z, Lee DH, Nguyen JT, Barbisin M, Xu NL, Mahuvakar VR, Andersen MR (2005) Real-time quantification of microRNAs by stem-loop RT-PCR. Nucleic Acids Res 33:e179. https://doi.org/10.1093/nar/gni178
23. Cissell KA, Rahimi Y, Shrestha S, Hunt EA, Deo SK (2008) Bioluminescence-based detection of microRNA, miR21 in breast cancer cells. Anal Chem 80:2319–2325. https://doi.org/10.1021/ac702577a
24. Válóczi A, Hornyik C, Varga N, Burgyán J, Kauppinen S, Havelda Z (2004) Sensitive and specific detection of microRNAs by northern blot analysis using LNA-modified oligonucleotide probes. Nucleic Acids Res 32:e175. https://doi.org/10.1093/nar/gnh171
25. Khoothiam K, Treerattrakoon K, Iempridee T, Luksirikul P, Dharakul T, Japrung D (2019) Ultrasensitive detection of lung cancer-associated miRNAs by multiple primer-mediated rolling circle amplification coupled with a graphene oxide fluorescence-based (MPRCA-GO) sensor. Analyst 144:4180–4187. https://doi.org/10.1039/C9AN00517J
26. Xu H, Lin Y, Sun L, Fang X, Jia L (2020) An integrated target recognition and polymerase primer probe for microRNA detection. Talanta 219:121302. https://doi.org/10.1016/j.talanta.2020.121302
27. Chen T, Xu Y, Wei S, Li A, Huang L, Liu J (2019) A signal amplification system constructed by bi-enzymes and bi-nanospheres for sensitive detection of norepinephrine and miRNA. Biosens Bioelectron 124–125:224–232. https://doi.org/10.1016/j.bios.2018.10.030
28. Wu Y, Li J, Quan K, Meng X, Yang X, Huang J, Wang K (2020) A DNAzyme cascade for amplified detection of intracellular miRNA. Chem Commun 56:10163–10166. https://doi.org/10.1039/D0CC02847A
29. Su J, Wang D, Nörbel L, Shen J, Zhao Z, Dou Y, Peng T, Shi J, Mathur S, Fan C, Song S (2017) Multicolor gold-silver nanomushrooms as ready-to-use SERS probes for ultrasensitive and multiplex DNA/miRNA detection. Anal Chem 89:2531–2538. https://doi.org/10.1021/acs.analchem.6b04729
30. Sun Y, Li T (2018) Composition-tunable hollow Au/Ag SERS nanoprobes coupled with target-catalyzed hairpin assembly for triple-amplification detection of miRNA. Anal Chem 90:11614–11621. https://doi.org/10.1021/acs.analchem.8b03067
31. Zhang X, Yang Z, Chang Y, Qing M, Yuan R, Chai Y (2018) Novel 2D-DNA-nanoprobe-mediated enzyme-free-target-recycling amplification for the ultrasensitive electrochemical detection of microRNA. Anal Chem 90:9538–9544. https://doi.org/10.1021/acs.analchem.8b02251
32. Su S, Sun Q, Ma J, Zhu D, Wang F, Chao J, Fan C, Li Q, Wang L (2020) Ultrasensitive analysis of microRNAs with gold nanoparticle-decorated molybdenum disulfide nanohybrid-based multilayer nanoprobes. Chem Commun 56:9012–9015. https://doi.org/10.1039/D0CC03845H
33. Wang X, Liu B, Xiao M, Zou Y, Lai W, Pei H, Alam MF, Zhang W, Wan Y, Li L (2020) Fractal SERS nanoprobes for multiplexed quantitative gene profiling. Biosens Bioelectron 156:112130. https://doi.org/10.1016/j.bios.2020.112130
34. Abolhasan R, Mehdizadeh A, Rashidi MR, Aghebati-Maleki L, Yousefi M (2019) Application of hairpin DNA-based biosensors with various signal amplification strategies in clinical diagnosis. Biosens Bioelectron 129:164–174. https://doi.org/10.1016/j.bios.2019.01.008
35. Choi JR, Hu J, Tang R, Gong Y, Feng S, Ren H, Wen T, Li X, Wan Abas WA, Pingguan-Murphy B, Xu F (2016) An integrated paper-based sample-to-answer biosensor for nucleic acid testing at the point of care. Lab Chip 16:611–621. https://doi.org/10.1039/C5LC01388G
36. Zhao Y, Chen F, Li Q, Wang L, Fan C (2015) Isothermal amplify cation of nucleic acids. Chem Rev 115:12491–12545. https://doi.org/10.1021/acs.chemrev.5b00428
37. Liu T, Gu M, Dong Y, Wang GL (2021) Methylene blue embedded duplex DNA as an efficient signal stimulator of petal-like $BiVO_4$ for ultrasensitive photoelectrochemical bioassay. Anal Chim Acta 1182:338945. https://doi.org/10.1016/j.aca.2021.338945
38. Nordin N, Yusof NZ, Abdullah J, Radu S, Hushiarian R (2016) Sensitive detection of multiple pathogens using a single DNA probe. Biosens Bioelectron 86:398–405. https://doi.org/10.1016/j.bios.2016.06.077
39. Su S, Hao Q, Yan Z, Dong R, Yang R, Zhu D, Chao J, Zhou Y, Wang L (2019) A molybdenum disulfide@methylene blue nanohybrid for electrochemical determination of microRNA-21, dopamine and uric acid. Microchim Acta 186:607. https://doi.org/10.1007/s00604-019-3678-0
40. DeSouza RM, Jones BR, Lowis SP, Kurian KM (2014) Pediatric medulloblastoma-update on molecular classification driving targeted therapies. Front Oncol 4:176. https://doi.org/10.3389/fonc.2014.00176

41. Khatua S, Song A, Citla Sridhar D, Mack SC (2018) Childhood medulloblastoma: current therapies, emerging molecular landscape and newer therapeutic insights. Curr Neuropharmacol 16:1045–1058. https://doi.org/10.2174/1570159X15666171129111324
42. Grunder E, D'Ambrosio R, Fiaschetti G, Abela L, Arcaro A, Zuzak T, Ohgaki H, Lv SQ, Shalaby T, Grotzer M (2011) MicroRNA-21 suppression impedes medulloblastoma cell migration. Eur J Cancer 47:2479–2490. https://doi.org/10.1016/j.ejca.2011.06.041